Earth and Planetary Science Letters 310 (2011) 9–20

Contents lists available at ScienceDirect

Earth and Planetary Science Letters

journal homepage: www.elsevier.com/locate/epsl

Changes in dip of subducted slabs at depth: Petrological and geochronological evidence from HP–UHP rocks (Tianshan, NW-China)

R. Klemd [a,*], T. John [b], E.E. Scherer [b], S. Rondenay [c,d], J. Gao [e]

[a] GeoZentrum Nordbayern, Universität Erlangen, Schlossgarten 5a, 91054 Erlangen, Germany
[b] Institut für Mineralogie, Universität Münster, Corrensstraße 24, 48149 Münster, Germany
[c] Department of Earth Science, University of Bergen, Allegaten 41, 5007 Bergen, Norway
[d] Department of Earth, Atmospheric, and Planetary Sciences, Massachusetts Institute of Technology, Cambridge, Massachusetts 02139 USA
[e] Institute of Geology and Geophysics, Chinese Academy of Sciences, P.O. Box 9825, Beijing, China

ARTICLE INFO

Article history:
Received 30 March 2011
Received in revised form 27 June 2011
Accepted 21 July 2011
Available online xxxx

Editor: T.M. Harrison

Keywords:
subduction
slab dip steepening
oceanic crust
Lu–Hf geochronology
(U)HP rocks
Tianshan

ABSTRACT

High-resolution seismic imaging has previously revealed sudden changes in the dip of subducted oceanic plates. This 'kinking' feature is crucial because in many subduction zones it is thought to coincide with the disappearance of the low-velocity layers associated with subducted oceanic crust. In this study, we present petrological evidence for this phenomenon derived from oceanic blueschist- and eclogite-facies rocks from the Chinese Tianshan. The investigated samples span a large range of peak metamorphic conditions, with temperatures between 330 and 580 °C at 1.5 to 2.3 GPa. Such variable peak metamorphic conditions, together with the intimate interlayering of high- and ultrahigh-pressure rocks, have also been reported from other Tianshan localities. These observations suggest that the rocks were derived from varying depths within the subduction zone and then juxtaposed during exhumation in the subduction channel. Multi-point Lu–Hf isochrons from four high-pressure rocks yield consistent garnet-growth ages of 313 ± 12, 315.8 ± 2.9, 313.9 ± 4.8, and 315.2 ± 1.6 Ma. These, in conjunction with the ~311 Ma cluster of published ^{40}Ar–^{39}Ar and Rb–Sr white mica ages from the same vicinities imply fast exhumation rates. The Lu–Hf ages confirm that the eclogite-facies metamorphism of the Tianshan high-pressure rocks occurred during a single subduction event in the Late Carboniferous. However, the previously reported peak metamorphic P-T estimates from UHP metasediments and eclogites all lie on a lower geothermal gradient – and thus on a colder P-T path at the slab-wedge interface – than the HP eclogites and meta-volcaniclastic rocks from this study. This suggests that the slab-subduction angle steepened sharply at a depth greater than approximately 90 km, i.e., between the depths at which the HP and UHP rocks equilibrated. In addition to the negative buoyancy of mafic UHP rocks in subduction zones, the kinking may act as a geometric hindrance to the exhumation of such rocks, thereby explaining their rarity.

1. Introduction

Eclogitization (dehydration) of subducting oceanic crust seems to coincide with the disappearance of the low-velocity layers found in seismic images of subduction zones (e.g., Rondenay et al., 2008; Yuan et al., 2000). Interestingly, some seismic images exhibit a change of dip or 'kinking' of subducting slabs near the depth of this transformation (e.g., Abers, 2005; Rondenay et al., 2001; Rondenay et al., 2008; Yuan et al., 2000). Thermodynamic reasoning implies that eclogitization of the oceanic crust would be nearly complete at the depth of the kink and that the related densification and stiffening would cause oceanic crust to become almost seismically indistinguishable from mantle peridotite (e.g., Rondenay et al., 2008; van Keken et al., 2011; Yuan et al., 2000). The large-scale deformation associated with the kinking of slabs seems to be localized where significant mineral reactions occur, most likely because of the positive feedback between mineral reactions and rock deformation at high pressures (e.g., Austrheim, 1987; John et al., 2009; Jolivet et al., 2005). Accordingly, if slabs are kinked, then this geometry should be recorded in the PTt evolution of the subducting rocks. Suites of high-pressure (HP) and ultrahigh-pressure (UHP) rocks from both above and below this purported kink are thus obvious targets for obtaining constraints on the geometry of subducting slabs.

The close association of exposed HP and UHP fragments of formerly subducted oceanic crust found in the Chinese Tianshan offer an excellent and as of yet unique possibility to reconstruct the PTt evolution of a subducting oceanic plate from HP to UHP conditions. We therefore performed a combined petrological and geochronological (Lu–Hf garnet) investigation on intimately associated HP rocks and discuss the results in the context of the existing knowledge about the Tianshan HP and UHP rocks. On the basis of the

* Corresponding author.
E-mail addresses: klemd@geol.uni-erlangen.de (R. Klemd), timm.john@uni-muenster.de (T. John), escherer@uni-muenster.de (E.E. Scherer), rondenay@MIT.EDU (S. Rondenay), gaojun@mail.igcas.ac.cn (J. Gao).

0012-821X/$ – see front matter © 2011 Elsevier B.V. All rights reserved.
doi:10.1016/j.epsl.2011.07.022

petrological and geochronological data from the HP rocks and from previously reported UHP rocks, we present a model that supports the existence of seismically inferred kinks in subducted slabs (e.g., Yuan et al., 2000; Rondenay et al., 2008).

2. Geological setting

The Tianshan orogen extends broadly east–west for about 2500 km from Uzbekistan, Tajikistan, Kyrgyzstan, and Kazakhstan to northwestern China and is situated along the southwestern margin of the Altaids or the Central Asia Orogenic Belt (CAOB)—(Sengör et al., 1993; Zonenshain et al., 1990; Fig. 1a). The Tianshan HP-LT metamorphic belt in NW China (Gao et al., 1995, 1998; Fig. 1a) represents a suture zone between the Yili (—Central Tianshan) and the Tarim blocks (Gao et al., 1999). It is mainly composed of blueschist, eclogite, greenschist-facies metasediments, and mafic meta-volcanic rocks, and it resembles typical mélanges (Gao and Klemd, 2003). The mafic rocks are chemically similar to typical oceanic basalts, such as N-MORB, E-MORB, OIB, and arc basalts (e.g., John et al., 2008). Blueschist occurs within greenschist-facies metasediments as small discrete bodies, lenses, bands, and as up to 4 km-thick layers (Fig. 1b). Eclogites are intercalated with the blueschist layers as pods, boudins, thin layers, or large massive blocks of almost 2 km^2 in plan view. The age of high-pressure metamorphism in the Tianshan has been suggested to be either Late Paleozoic (e.g., Gao et al., 1995, 1998; Gao and Klemd, 2003; Hegner et al., 2010; Klemd et al., 2005; Simonov et al., 2008; Stupakov et al., 2004; Su et al., 2010) or Triassic (Zhang et al., 2007). Most eclogites underwent peak metamorphism estimated to range between 480 and 580 °C at 1.8–2.3 GPa on a regional scale (e.g., Klemd et al., 2002; Lin and Enami, 2006; Lü et al., 2007). Peak UHP metamorphic conditions – confirmed by the presence of coesite – of 2.5–2.7 GPa at 420–520 °C have been reported for a single eclogite boudin (Lü et al., 2009) that is entirely enclosed by pelitic–felsic schists that display variable peak metamorphic conditions ranging from HP to UHP. Pseudosection modeling of the pelitic–felsic schists yielded pressures of 2.8–3.2 GPa at 550–570 °C, 2.2–2.4 GPa at 480–550 °C, and 2.1–2.3 GPa at 530–550 °C (Lü et al., 2008; Wei et al., 2009). Other eclogite boudins from this locality show pressures from 1.8 to 2.5 GPa at temperatures between 400 and 600 °C (Lü et al., 2007). Wei et al. (2009) stated that the '*Tianshan eclogite belt is dominated by HP pelitic–felsic schists …, but contains UHP slices or blocks…*' whereas Lü et al. (2009) suggested that eclogite-facies rocks have been detached from different depths of the slab and mixed on a meter scale within the subduction channel during exhumation. The latter is in agreement with the basic concept for the Tianshan of van der Straaten et al. (2008) and numerical modeling studies, which suggested that UHP and HP continental terranes as well as subducted HP mafic oceanic crust were exhumed as mélanges. Thus, HP and UHP rocks of such mélanges underwent metamorphism at different pressures and temperatures (i.e., complex and different P-T trajectories) despite their common origin from one subduction plate (e.g., Gerya et al., 2002; Gerya et al., 2008; Gerya and Stöckhert, 2006; Li and Gerya, 2009; Warren et al., 2008a,b; Yamato et al., 2007).

To obtain further petrological and geochronological information on the high-pressure metamorphism and thus the collision of the Yili-Central zone terrane and the Tarim block, four high-pressure mafic meta-volcanic (FTS 9–3) and meta-volcaniclastic (FTS 9-2, 9-4, and 5-15) samples from the western Tianshan HP-LT belt (Fig. 1b) were selected for Lu–Hf garnet dating.

3. Analytical methods

Whole rock samples were crushed with a steel jaw crusher and then powdered in an agate mill. Garnet and omphacite were separated using a steel jaw crusher, a disk mill, a magnetic separator, and handpicking. Major elements were measured by X-ray-fluorescence analysis (XRF, Phillips PW 1480) on fused glass disks at the Institute für Geowissenschaften, Universität Kiel. Accuracy and precision are

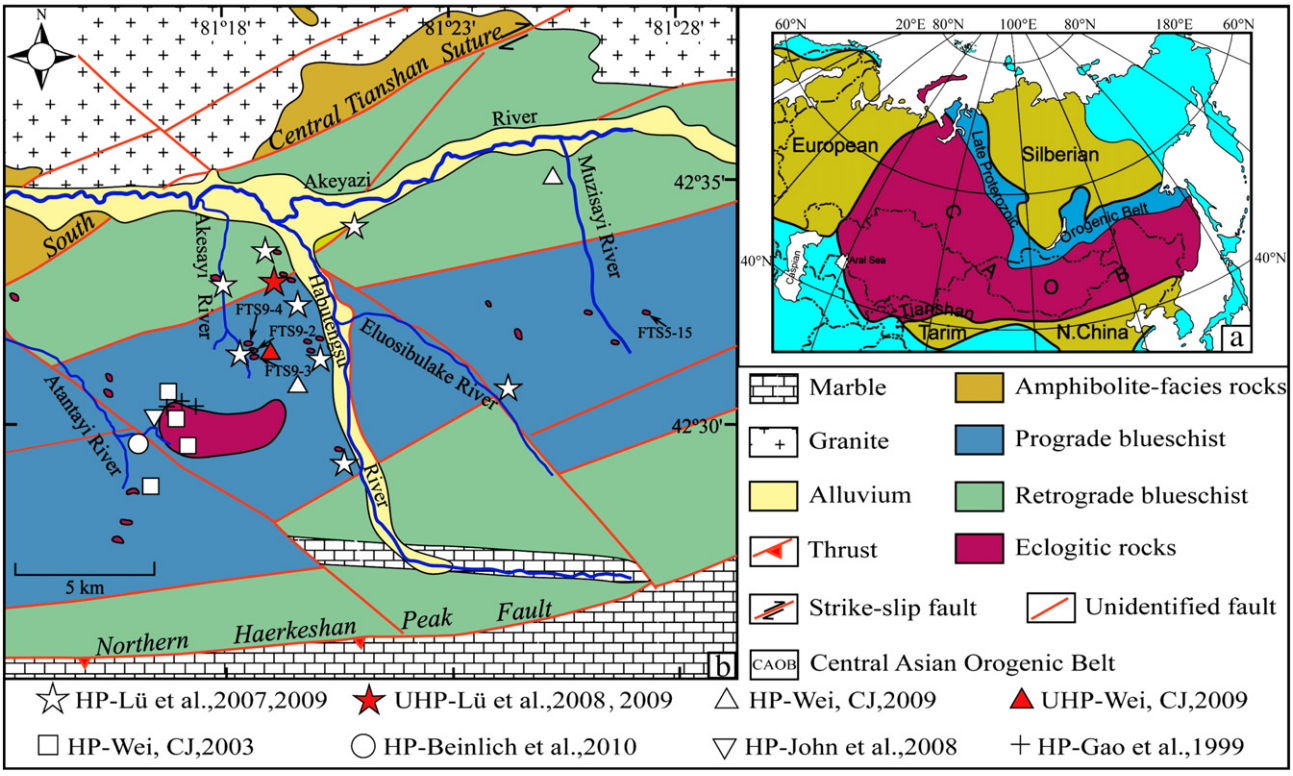

Fig. 1. Geological map of the western Tianshan high-pressure, low-temperature metamorphic belt in northwestern China showing sample localities (modified after Gao et al., 1995, 1999).

better than 1% RSD for the major oxides (see van der Straaten et al., 2008 for analytical details). Trace element compositions were obtained on the same fused glass disks by LA–ICPMS analysis at the GeoZentrum, Universität Erlangen. The instrument used was a single collector quadrupole AGILENT 7500i ICP-MS equipped with a 266 nm Merchantek LUV 266x laser. Bulk-rock SiO_2 was used to normalize the LA–ICP-MS analyses. The glass reference material NIST SRM 612 and the values of Pearce et al. (1997) were used for external calibration and calculation of trace element concentrations. The data were processed using the GLITTER Version 3.0 online interactive data reduction for LA–ICP-MS by Macquarie Research Ltd. Reproducibility, accuracy, and precision of the method were monitored by repeated analysis of NIST SRM 614 and whole rock standards (e.g., Jochum et al., 2006). The precision of REE, Nb, Ta, and Th concentrations is better than 5% (1 σ), except for Gd and Er (5–8%). See Schulz et al. (2006) for additional LA–ICP-MS details.

Major element mineral analyses were obtained with a JEOL JXA8600MX at the Institut für Mineralogie, Universität Münster and a JEOL JXA82000 at the GeoZentrum Nordbayern, Universität Erlangen. Operating conditions for both were a 15 kV acceleration voltage, a 15 nA beam current, and a counting time of 10 s. The beam diameter was 3–5 μm. Natural mineral standards were used. The analytical error is 1–2% RSD. The raw data were corrected with a ZAF procedure.

The Lu–Hf isotope analyses were conducted at the Zentrallabor für Geochronologie at the University of Münster. All samples were spiked with a mixed ^{180}Hf–^{176}Lu tracer before digestion. Whole rock powders were decomposed with HF–HNO_3 in steel-jacketed Teflon bombs for 5 days at 180 °C, and then evaporated with $HClO_4$ to break down fluorides. This procedure dissolves refractory Hf-bearing phases, e.g., zircon and rutile. Such phases, when significantly older or younger than the HP parageneses, may adversely affect Lu–Hf isochron ages (e.g., Scherer et al., 2000). For this reason, whole rock chips and mineral separates (garnet and omphacite grains) were digested using a "tabletop" method that avoids dissolving zircon and rutile while completely dissolving the mineral(s) of interest (e.g., Lagos et al., 2007). This entails alternating treatments with HF-HNO_3-$HClO_4$ and 10 M HCl in capped Savillex vials on a 120 °C hotplate, uncapping and drying the samples down at ~180 °C between these steps. This procedure was repeated until no visible vestiges of the target minerals remained, and then performed once more to ensure equilibration of the tracer with the dissolved portion of the sample. After sample decomposition, samples were dissolved in ~5 ml of 6 M HCl and diluted to 3 M HCl with Milli-Q water (18.2 MΩ-cm). The sample solutions were then centrifuged and loaded onto ion exchange columns containing Ln-Spec resin. The separation of Lu and Hf from the sample matrix follows that of Münker et al. (2001). The resulting Hf and Lu fractions were processed again through the chemistry, but loading in 3 M HCl–0.1 M ascorbic acid (Sprung et al., 2010). This additional step removes any remaining iron and ensures that the Hf cut is free of (spiked) lutetium. The total procedural blanks averaged 2.5 pg and 153 pg for Lu and Hf, respectively. Lutetium and Hf were analyzed in static mode on the Micromass Isoprobe in Münster. The Hf data were corrected for instrumental mass bias using the exponential law and $^{179}Hf/^{177}Hf = 0.7325$. The $^{176}Hf/^{177}Hf$ values are reported relative to 0.282160 for our in-house standard, which isotopically identical to the JMC-475 standard. For isochron regressions, the expected external (2 s.d.) reproducibility of samples that could only be analyzed once was estimated using the reproducibility of standard solutions analyzed at different signal intensities (Bizzarro et al., 2003). The Lu analyses were precisely corrected for isobaric interference from ^{176}Yb using the method of Blichert-Toft et al. (2002), whereas the mass bias correction was made by monitoring the $^{187}Re/^{185}Re$ of admixed rhenium (Scherer et al., 2001). This results in an external precision of ~0.2% for the $^{176}Lu/^{177}Hf$ values for optimally spiked samples. To calculate ages, a ^{176}Lu decay constant of 1.867×10^{-11} yr^{-1} was used (mean of data from Scherer et al., 2001, 2003; Söderlund et al., 2004). The spatial distribution of Lu within representative garnet porphyroblasts was determined by laser ablation and inductively coupled plasma mass spectrometry (LA–ICP-MS) in Münster. Element profiles were made across the crystals in polished thin sections. Sample ablation was done with a pulsed 193 nm ArF excimer laser (UP193HE, New Wave Research) at a repetition rate of 5 Hz and an energy of ~9 J/cm^2. The beam spot diameter was 25 μm. Elemental analysis was carried out with an Element2 mass spectrometer (ThermoFisher). The forward power was 1250 W and the gas flow rates were 0.6 L/min for the He carrier gas, and 1.2 L/min and 1 L/min for the Ar-auxiliary and sample gas, respectively. The cooling gas flowed at 16 L/min. Before starting with analyses, the torch position, lenses, and gas flows were tuned during the ablation of NIST SRM 612 glass to obtain stable ^{139}La, ^{232}Th, and $^{232}Th^{16}O$ signals, high ^{139}La and ^{232}Th sensitivity, and low oxide rates ($^{232}Th^{16}O/Th^{232}$ <0.1%). Twenty elements were analyzed using the NIST 612 glass as the external standard and Si as the internal standard. Each analysis lasted 60 s (20 s for background, 40 s sample signal after switching laser on). Concentrations of measured elements were calculated using the Glitter software.

4. Petrography

Three of the four samples which were chosen for the detailed petrological and Lu–Hf garnet geochronological study were taken along the southern part of the Akesayi River (N 42°30′59.4″/E 081°18′ 49,6″ FTS 9-2, 9-3, and 9-4) and the fourth one at the southern part of the Muzisayi River and (N 42°32′14.1″/E 081°27′08.4″ FTS 5-15; Fig. 1b).

The mafic meta-volcanic sample (FTS 9-3) is massive in character and stems from an outcrop that locally preserved some pillow structures. Two meta-volcaniclastic samples (FTS 9-2 and 9-4) enclose the mafic metavolcanic rocks. Three of the samples (FTS 9-2, 9-3, and 9-4) are prograde eclogites (sensu lato) characterized by prograde growth features in their mineral assemblages and lack of a significant retrograde overprint. None of these rocks was completely transformed to eclogite sensu stricto (i.e., garnet + omphacite >70 vol.%, Carswell, 1990) but all contain the critical mineral eclogite-facies mineral assemblage (omphacite + garnet + rutile) and have a massive, granoblastic texture and are hereafter termed eclogites. Sample FTS 5–15 is a blueschist-facies garnet-glaucophane-albite schist that displays a strong blueschist- to greenschist-facies retrograde overprint. The concentrations of the major, trace, and rare earth elements in the four samples (Table Supplement S-1) correspond to a basaltic to andesitic composition.

4.1. Eclogite

Texturally peak metamorphic omphacite, garnet, clinozoisite, paragonite, rutile, and quartz are present in all three samples (Table S-2). Sample FTS 9-2 is the only one that contains prograde, idioblastic glaucophane. In FTS 9-4, glaucophane only occurs as inclusions in garnet. Sample FTS 9-3 contains neither peak-metamorphic glaucophane nor Ca–Na amphibole, apart from glaucophane inclusions in garnet. Minor phases include chlorite, titanite (replacing rutile), carbonate, pyrite, and other opaque minerals. All three samples have a massive granoblastic texture. Subidioblastic to idioblastic garnet grains vary between 0.2 and 5 mm across in samples FTS 9-3 and 9-2. Typical inclusions in garnet cores are glaucophane or Ca–Na-amphibole, omphacite, paragonite, clinozoisite, quartz, titanite, rutile, albite, chlorite, and carbonate, whereas garnet rims in all samples are generally inclusion-free. In contrast to the other two samples, garnet porphyroblasts in sample FTS 9-4 are finer-grained (<0.5 mm) with rare, usually submicroscopic inclusions in their cores. As was previously observed for eclogites from other localities in the Tianshan,

box-shaped clinozoisite-paragonite-albite intergrowths occur in garnet cores of sample FTS 9-3, suggesting the former presence of lawsonite (see Klemd et al., 2002). Randomly oriented fibroblastic omphacite generally occurs in the sub-millimeter range. Paragonite and phengite cannot be distinguished optically or from their textural context in the matrix of samples FTS 9-3 and 9-4.

4.2. Albite-glaucophane-garnet-schist

This rock (FTS 5-15) has a well-developed foliation defined by aligned paragonite and glaucophane crystals. Late albite porphyroblasts are also aligned, indicating that the foliation developed during exhumation. The peak assemblage of the sample consists of garnet, glaucophane, rutile, quartz, and paragonite (Table S-2). Post-peak minerals are albite and accessory titanite, carbonate, zircon, and opaque phases.

The idioblastic to subidioblastic garnet porphyroblasts typically contain inclusions of monocrystalline quartz, rutile, and (rarely) carbonate. Box-shaped clinozoisite and paragonite inclusions in the garnet cores again suggest the former presence of lawsonite. Most of the quartz inclusions occur in the garnet rims. The pressure shadows of the garnet porphyroblasts contain glaucophane and/or Ca-amphibole, paragonite, and titanite, all of which have been replaced or mantled by coarse-grained albite. Idioblastic glaucophane has often been replaced by Ca-amphibole, and both occur as oriented inclusions in albite and clinozoisite. The glaucophane and Na–Ca-amphibole inclusions are locally optically continuous, suggesting that they were part of a single crystal before porphyroblastic albite growth.

5. Mineral chemistry

Representative mineral chemical compositions are given in Tables S-3–7. The mineral compositions used for geothermobarometry are listed in Table 1.

5.1. Garnet

The eclogitic garnet idioblasts have an average core and rim composition of $Alm_{67-74}Pyr_{5-14}Grs_{21-24}Spess_{1.5-2.3}$ and $Alm_{58-67}Pyr_{5-12}Grs_{19-33}Spess_{1-1.5}$, respectively (Table 1; Table S-3). They show an almost constant, monotonic $Fe^{2+}/(Fe^{2+}+Mg)$, which decreases slightly at the outermost rims while the grossular component increases (Fig. S-1). The spessartine component decreases while the pyrope component slightly increases from core to rim. Due to bulk rock chemical differences, the garnet porphyroblasts from the blueschist (FTS 5-15) have a somewhat different chemistry with an average core composition of $Alm_{57-73}Pyr_{3-7}Grs_{17-19}Spess_{2-19}$ and rim composition of $Alm_{56-61}Pyr_{7-10}Grs_{28-34}Spess_{0.2-0.3}$. However, some of these garnet porphyroblasts (Table S-3) display similar zoning patterns to those of garnet in the eclogites, i.e., they have a large, homogeneous core with grossular and pyrope components increasing and almandine and spessartine contents slightly decreasing toward the outermost rim (Fig. S-1). The overall continuous, monotonic compositional zoning of X_{Fe} is displayed by most grains (Fig. S-1). Zoning in X_{Mn} defines a 'bell-shaped' profile (Fig. S-1), which we consider to have resulted from fractionation-depletion during prograde garnet growth (Hollister, 1966). In general, the Ca-content shows a strong increase from a relatively homogeneous core to the rim, accompanied by a decrease of Mn (Fig. 2). However, even though the cores have the highest Mn concentrations, there is always a chemically sharp boundary toward the outer parts of the garnet grains (Fig. 2). We interpret this feature as evidence for changes in the element supply during prograde garnet growth and a lack of diffusional equilibration during retrograde conditions. In addition, the presence of sharp chemical boundaries and the lack of irregularities such as embayments between core and rim suggest that no garnet resorption occurred before the growth of the garnet rims. In two dimensions, garnet crystals from FTS 5-15 show a very distinct prograde zonation from core to rim (Fig. 2j, k) with X_{Ca} and X_{Mn}

Table 1
Mineral compositions used for geothermobarometry of HP rocks from the western Tianshan, NW China.

Mineral compositions used for geothermobarometry														
	Garnet								Omphacite				Phengite	
Sample	FTS 9-2	FTS 9-2	FTS 9-3	FTS 9-3	FTS 9-4	FTS 9-4	FTS 9-2	FTS 9-2	FTS 9-3	FTS 9-3	FTS 9-4	FTS 9-4	FTS 9-3	FTS 9-4
Profile	rGrt1/4 rim	Grt2/8 rim	Grt3 rim	Grt1 rim	Grt2 rim	Grt2 rim	omp4 p6	omp5	omp3 p5	omp1 p3	bse3 p16	cpx1 p1	mica2 p5	mic2 p3
SiO2	38.29	38.08	37.82	38.12	37.59	37.78	55.92	54.82	55.06	54.71	56.21	56.01	54.44	53.32
TiO2	0.06	0.04	0.092	0.01	0.01	0.00	0.05	0.13	0.20	0.14	0.11	0.01	0.23	0.21
Al2O3	20.99	21.22	21.85	21.96	21.88	21.88	10.12	10.60	8.88	8.54	12.77	12.48	23.66	22.12
Cr2O3	0.01	0.00	0.00	0.00	0.00	0.00	0.00	0.01	0.02	0.00	0.00	0.00	0.03	0.00
FeO	29.81	28.28	27.19	26.46	27.30	28.84	8.79	8.83	12.30	12.18	3.81	3.94	3.71	2.00
MnO	0.15	0.15	0.501	0.51	0.26	0.56	0.01	0.00	0.00	0.04	0.00	0.03	0.00	0.00
MgO	2.46	2.41	1.61	1.66	3.61	3.17	5.86	5.43	4.58	4.80	6.88	7.02	3.66	4.72
CaO	8.61	10.29	11.66	11.77	8.81	7.73	11.39	10.78	10.51	10.82	11.28	11.59	0.04	0.00
Na2O	n.a.	n.a.	n.a.	n.a.	n.a.	n.a.	7.99	8.04	8.42	8.17	8.47	8.22	0.18	0.28
K2O	n.a.	n.a.	n.a.	n.a.	n.a.	n.a.	0.04	0.01	0.00	0.00	0.00	0.00	10.38	10.38
Total	100.39	100.47	100.73	100.49	99.46	99.96	100.17	98.64	99.96	99.40	99.53	99.30	96.33	93.03
Si	6.06	6.00	5.95	6.00	5.94	5.98	2.00	1.99	2.00	2.00	1.99	1.99	3.60	3.63
Ti	0.01	0.01	0.01	0.00	0.00	0.00	0.00	0.00	0.01	0.00	0.00	0.00	0.01	0.01
Al	3.91	3.94	4.05	4.07	4.07	4.08	0.43	0.45	0.38	0.37	0.53	0.52	1.84	1.77
Cr	0.00	0.00	0.00	0.00	0.00	0.00	0.00	0.00	0.00	0.00	0.00	0.00	0.00	0.00
Fe3+	0.00	0.04	0.02	0.00	0.03	0.00	0.12	0.12	0.21	0.21	0.07	0.07	n.c.	n.c.
Fe2+	3.95	3.69	3.56	3.48	3.58	3.82	0.14	0.15	0.16	0.16	0.04	0.05	0.20	0.11
Mn	0.02	0.02	0.07	0.07	0.04	0.08	0.00	0.00	0.00	0.00	0.00	0.00	0.00	0.00
Mg	0.58	0.57	0.38	0.39	0.85	0.75	0.31	0.29	0.25	0.26	0.36	0.37	0.36	0.48
Ca	1.46	1.74	1.97	1.99	1.49	1.31	0.44	0.42	0.41	0.42	0.43	0.44	0.00	0.00
Na	n.a.	n.a.	n.a.	n.a.	n.a.	n.a.	0.56	0.57	0.59	0.58	0.58	0.57	0.02	0.04
K	n.a.	n.a.	n.a.	n.a.	n.a.	n.a.	0.00	0.00	0.00	0.00	0.00	0.00	0.87	0.90
Sum_cat	16.00	16.00	16.00	16.00	16.00	16.00	4.00	4.00	4.00	4.00	4.00	4.00	6.92	6.94

n.a. = not analyzed.
n.c. = not calculated.
Garnet calculated on the basis of O = 24.
Omphacite calculated on the basis of O = 6.
Phengite calculated on the basis of O = 11.

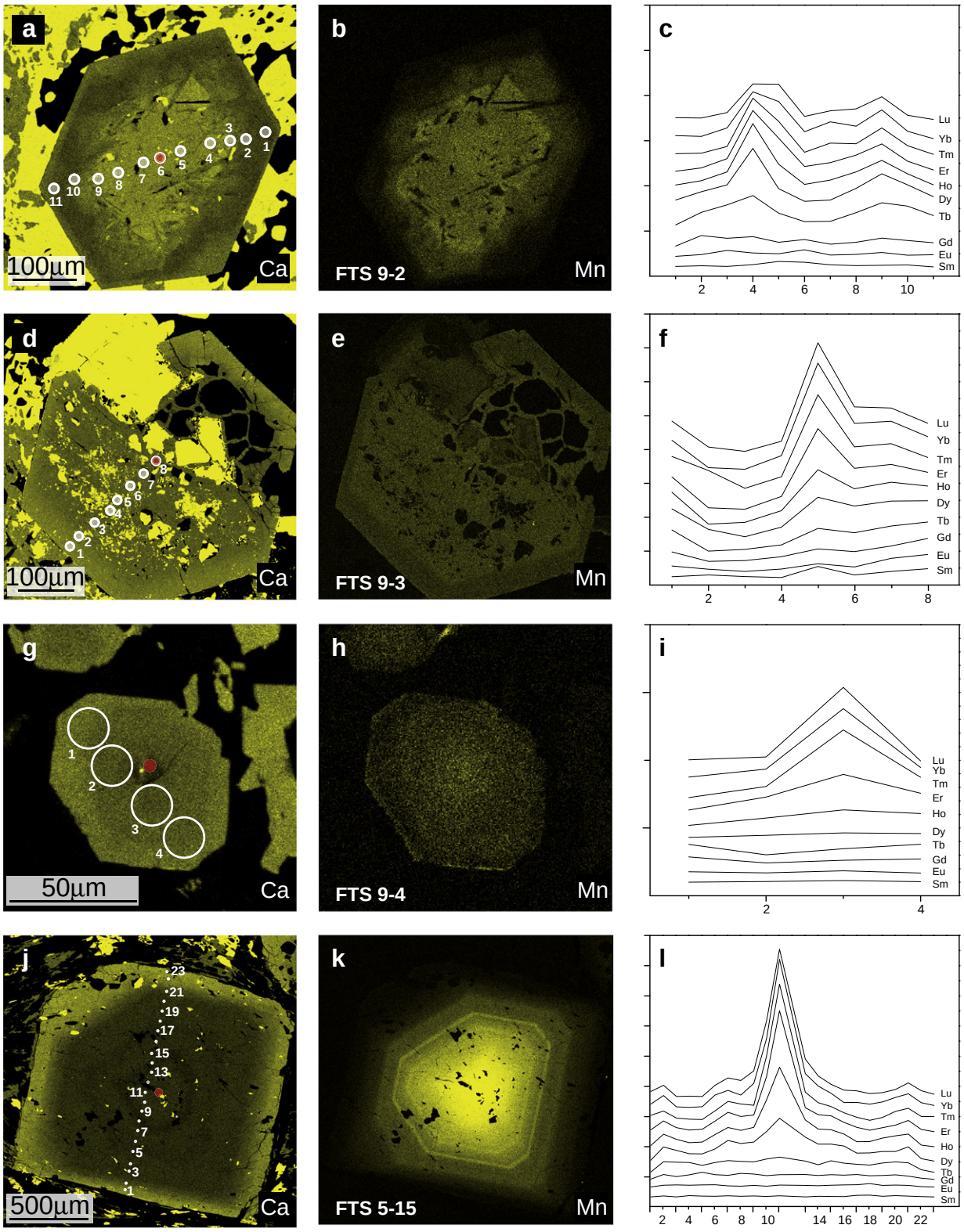

Fig. 2. Element maps of garnet porphyroblasts showing a) X_{Ca} and b) X_{Mn} of FTS 9-2 (garnet diameter = 300 µm), d) X_{Ca} and e) X_{Mn} of FTS 9-3 (garnet diameter = 500 µm), g) X_{Ca} and h) X_{Mn} of FTS 9-4 (garnet diameter = 70 µm), j) X_{Ca} and k) X_{Mn} of FTS 5-15 (garnet diameter = 400 µm), (light = high concentration, dark = low concentration (see text for details). Circles on the Ca maps indicate spot positions for REE analysis by LA–ICPMS; red spots indicate grain centers. Chondrite-normalized REE profiles (c, f, i, l) are plotted on a log scale, and have been stacked for clarity. Each y-axis tick corresponds to half an order of magnitude; ticks on x-axes correspond to the spot numbers.

displaying prominent oscillatory changes that do not coincide with the spatial distribution of inclusions. Thus volume diffusion was hampered by low time-integrated temperature. All studied porphyroblasts, except that from FTS 9-3, show a more pronounced zoning in HREE as compared to the middle rare earth elements (MREE). The HREE are either broadly distributed over the garnet cores (garnet FTS

9-2, Fig. 2c) or display sharp decreases from core to rim (FTS 9-3 and 5-15; Fig. 2f, l). The Lu profile in garnet FTS 5-15 (Fig. 2l) is suggestive of Rayleigh fractionation during garnet growth. This commonly is interpreted to be a result of core-to-rim prograde growth (e.g., Otamendi et al., 2002) and is in accordance with the behavior of the major elements.

5.2. Clinopyroxene

Using the classification of Morimoto et al. (1988), all investigated clinopyroxene grains are omphacite, with jadeite components ranging between 40 and 57 mol% (Table 1, Table S-4; Fig. S-2). No systematic chemical zoning was observed within single grains. Omphacite inclusions in garnet have compositions similar to those in the immediately adjacent matrix, suggesting fast garnet growth during prograde metamorphic conditions where local equilibrium was maintained at <cm scales. However, within a thin section, the clinopyroxene chemistry varies somewhat among different domains, indicative of bulk disequilibrium on a ~cm scale.

5.3. Amphibole

Selected analyses are given in Table S-5. In general, the texturally primary amphiboles are Na-amphibole that has been partially replaced by retrograde Ca–Na amphiboles (classification of Leake, 1978; Fig. S-3). The Na-amphibole is either glaucophane or ferro-glaucophane, whereas Ca–Na amphibole includes barroisite and ferro-barroisite. In sample FTS-9-4, magnesio-hornblende seems to replace omphacite on rare occasions. In sample FTS 5-15, glaucophane has been locally replaced by magnesio-hornblende as a result of decompression.

5.4. White mica

All samples contain paragonite having a Si-content between 3.06 and 3.11 a.p.f.u. and a Na-content between 0.75 and 0.88 a.p.f.u. (Table 1, Table S-6). No compositional differences were detected between matrix paragonite and paragonite inclusions in garnet. The Si-content of phengite varies between 3.30 and 3.62 a.p.f.u (Table S-6).

5.5. Other minerals

The representative composition of other investigated minerals such as clorite, clinozoisite, albite, and titanite are shown in Table S-7.

6. Metamorphic evolution

The presence of box-shaped pseudomorphs of clinozoisite, paragonite, albite, and quartz inclusions in garnet suggests that lawsonite-blueschist facies conditions (Evans, 1990) prevailed during burial of samples FTS 9-2, 9-3, and 5-15. The absence of kyanite and the presence of paragonite in the peak metamorphic mineral assemblage of all 4 samples provides a maximum H_2O-dependent pressure of 2.0 to 2.5 GPa at 350 to 550 °C, respectively, using the univariant reaction $Pg = Omph_{Jd57} + Ky + H_2O$. An H_2O-independent pressure estimate can be made from the reaction $Ab = Jd + Qtz$ (Holland, 1980). In the absence of (peak metamorphic) albite, the maximum jadeite content of 57 mol% indicates minimum pressures of 0.9 to 1.6 GPa at 350 to 550 °C, respectively. Peak metamorphic conditions were obtained from the temperature and pressure dependent Fe–Mg and Tschermaks exchange among garnet, omphacite, and phengite (Krogh-Ravna, 2000; Waters, 1996). Rim compositions of garnet (Table 1) were used in combination with the compositions of matrix omphacite (not touching, Table 1) and matrix phengite (close to garnet and having the highest Si content, Table 1) to calculate P-T conditions. Estimated peak P-T conditions vary among the investigated samples. Sample FTS 9-3 reached a maximum pressure of 2.0 to 2.4 GPa at 540 to 600 °C (6 mineral pairs), whereas sample FTS 9-4 reveals 1.5–1.9 GPa at 330 to 430 °C (6 mineral pairs). Temperatures of 500 to 580 °C at 1.6 to 2.0 GPa were calculated for sample FTS 9-2 (4 mineral pairs). Estimated temperatures based on the calibration of Ellis and Green (1979) are consistently 50 to 90 °C higher for most samples. The absence of omphacite in blueschist FTS 5-15 suggests that peak metamorphism for this sample was only blueschist-facies and never reached eclogite-facies. The chemical similarities between samples FTS 9-4 and 5-15 (see Table S-1) rule out a different bulk composition (e.g., low Na and/or Ca) as an explanation for the lack of omphacite crystallization during the prograde metamorphism of FTS 5-15. That peak P-T conditions vary among samples is surprising considering that they were collected from within a small area (Fig. 1b) and were not separated by major faults or shear zones. However, a similar phenomenon has been reported from other localities in the Chinese western Tianshan HP-LT belt, where Lü et al. (2007, 2008) observed high- and ultrahigh-pressure eclogites and metasediments that were intimately interlayered on a meter-scale. Another problem is the absence of lawsonite, which should have been stable under the calculated peak P-T conditions of 330 to 430 °C at 1.5–1.9 GPa in sample FTS 9-4 (e.g., Clarke et al., 2006; Ravna et al., 2010). Even at somewhat higher temperatures, the absence of lawsonite from the peak-metamorphic mineral assemblage is thought to stem from its breakdown during exhumation or an unfavorable bulk chemical composition. When plotting the peak metamorphic estimates in a P-T diagram however, all HP rocks investigated here, together with previously studied Tianshan HP and UHP rocks, lie on two different P-T trajectories and geothermal gradients (Fig. 3). Selected P-T estimates for HP and UHP rocks from the Chinese Tianshan are given in Table 2.

7. Geochronology

The Lu–Hf data and corresponding isochrons for the four high-pressure rocks are presented in Table 3 and Fig. 4. Isochron data were regressed using Isoplot/Ex version 3.72 (Ludwig, 2008), and the 2 s.d. external uncertainties for $^{176}Lu/^{177}Hf$ and $^{176}Hf/^{177}Hf$ that were estimated as explained above in the analytical methods. The three meta-volcaniclastic rocks define relatively precise Carboniferous ages: A seven-point isochron from sample FTS 9-2, which includes four garnet fractions, an omphacite fraction, and two whole rock fractions (tabletop chips and bombed powder), yields an age of 315.8 ± 2.9 Ma (MSWD = 0.83, all reported age uncertainties are 95% confidence limits). For sample FTS 9-4, all six fractions (three garnet, one omphacite, plus the tabletop wr chips and bombed wr powder) gave an age of 313.9 ± 4.8 Ma (MSWD = 1.8). The Lu–Hf data for FTS 5-15 (seven garnet fractions, two bombed whole rock aliquots, a bombed, garnet-poor matrix mineral fraction, and an aliquot of table-top digested whole rock chips) show somewhat more scatter, yielding 314.9 ± 1.9 Ma (MSWD = 5.2), or, if the tabletop-digested whole rock is excluded from the regression, 315.2 ± 1.6 Ma (MSWD = 3.3). Two garnet fractions, the omphacite, and the bombed whole rock of mafic meta-volcanic sample FTS 9-3 gave an age consistent with those of the other three samples, albeit with larger uncertainty: 313 ± 12 Ma. The weighted mean age of all four samples is 315.2 ± 1.3 Ma.

Whole rocks were digested both as powders, using high-pressure autoclaves ("bombs") and, except for FTS 9-3, as coarsely crushed chips (1–5 mm) using the low-pressure tabletop procedure described in the analytical methods. This was done to test for the presence of any zircon (or rutile) in the rock that formed either significantly before or after the appearance of the high-pressure garnet + omphacite assemblage and would therefore bias the age (Scherer et al., 2000). The bomb digestions should have dissolved all zircon and rutile, whereas the tabletop digestions of rock chips often result in little or no dissolution of those low-Lu/Hf refractory minerals, lessening their affect on the data point. This results in the tabletop-digested whole

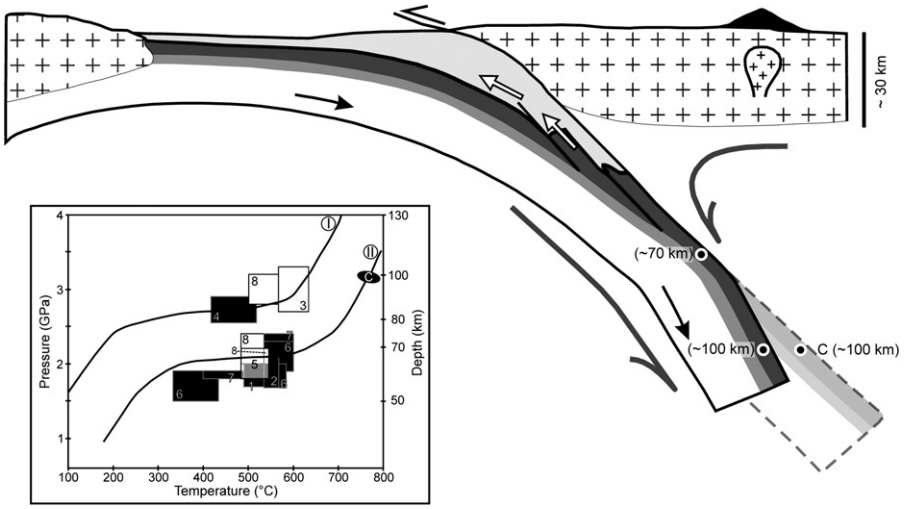

Fig. 3. Schematic illustration of a subduction zone in an oceanic-continental margin setting (modified after Agard et al., 2009) showing a dip angle that steepens at >90 km depth (i.e., UHP conditions). In addition, approximate locations of high-(from ~70 km depth) and ultrahigh-pressure (from ~100 km depth) rocks from the Tianshan are shown. C marks a possible location of ultrahigh-pressure rocks from a subduction zone in which there is no slab kink at depth. Inset: P-T diagram showing the predicted P-T trajectories for the West Aleutians (II) and the Central Honshu (I) subduction slab interfaces when using high-resolution finite element models employing non-Newtonian rheologies as examples of cold and hot subduction zones from the North Pacific plate (Syracuse et al., 2010). The P-T data for the eclogites and blueschists (black rectangles) and for the metasediments (open rectangles) are from (1) Klemd et al. (2002), (2) John et al. (2008), (3) Lü et al. (2009), (4) Lü et al. (2008), (5) Beinlich et al. (2010), (6) the present study, (7) Lü et al. (2007), and (8) Wei et al. (2009) (see also Table 2). It is evident that the Tianshan peak HP (~70 km depth) and UHP (~100 km) data depth plot on different trajectories (I and II).

rocks having lower Hf contents and higher Lu/Hf than those of the corresponding bomb-digested samples (Table 3). Any significant effects stemming from zircon (±rutile) that was either inherited or formed during a post-eclogite stage would result in the bombed whole rocks (or matrix) plotting off of isochrons defined by the tabletop-digested minerals. For all samples that we tested in this manner (FTS 9-2, 9-4, and 5-15), there was no clearly resolvable age difference between isochrons defined using only the bombed whole rock and those defined using only tabletop-digested whole rock. For FTS 9-3, excluding the bomb-digested whole rock from the regression does not change the sample's age significantly, but lowers the scatter (315.8 ± 4.9 Ma, MSWD = 1.7; cf. 313 ± 12 Ma, MSWD = 2.3). Thus any inherited- or post-eclogite zircon (±rutile) components in these rocks must be either similar in age to the eclogitization or minor in abundance relative to eclogite-stage zircon (±rutile).

8. Discussion and conclusions

8.1. Pressure-temperature-time paths

The four high-pressure samples of this study record a wide range of peak metamorphic conditions, from ca. 330 to 600 °C at about 1.6 to 2.4 GPa. This, together with their intimate occurrence indicates that they were derived from different depths in the subduction zone or within the slab and then juxtaposed during exhumation within the subduction channel (e.g., Lü et al., 2009; van der Straaten et al., 2008).

The relatively low peak temperatures are interpreted to be responsible for the excellent preservation of prograde growth features, including sharp Mn zoning in garnet crystals (Fig. 2). Because Mn^{2+} is expected to diffuse faster than Lu^{3+} and Hf^{4+} in garnet (e.g., Van Orman et al., 2002), but still exhibits such sharp zoning, we infer that the closure temperature of Lu–Hf in garnet has not been exceeded and that the Lu–Hf ages therefore date prograde garnet growth. If the crystallization interval was sufficiently long, the cores of porphyroblasts would be measurably older than the rims, and the Lu–Hf age of the bulk garnet would be weighted according to Lu concentration of the concentric growth zones (Lapen et al., 2003). To estimate the effect that a prolonged growth interval would have on our measured ages, we used the measured Lu concentration profiles from the porphyroblasts and modeled Lu concentration in spherical porphyroblasts. Assuming a maximum interval of 10 Ma and a constant crystal growth rate (volume/time), we find that our measured ages would exceed the true average age of the entire garnet volume by 0–2 Ma at most. For all four dated rocks, this small bias is within the quoted age uncertainties, and we take the apparent Lu–Hf ages to represent the stage in HP garnet growth at which about half of the garnet volume was present. Note that even the pronounced Lu concentration peak in the core of the FTS 5-15 garnet (Fig. 2l) only produces a small bias toward the core age; i.e., such Lu patterns do not necessarily indicate that Lu–Hf would date the start of garnet nucleation.

The consistency of Lu–Hf ages (~315 Ma) indicates that all samples – though derived from the subducting slab at different depths – have undergone high-pressure metamorphism at approximately the same time. Exhumation followed soon afterwards as indicated by the ~311 Ma ^{40}Ar–^{39}Ar ages and 313–302 Ma Rb–Sr ages of white mica (e.g., Klemd

Table 2
Selected prograde eclogite-facies P-T estimates based on conventional geothermobarometry and quantitative phase diagrams.

Source	*P* (Gpa)	Method	T (°C)	Method	Nr.[a]
Conventional geothermobarometry					
Klemd et al. (2002)	1.9 ± 0.2	Grt-Cpx-Phen	490–570	Grt-Cpx[b]	(1)
John et al. (2008)	1.9 ± 0.2	Grt-Cpx-Phen	530–560	Grt-Cpx[b]	(2)
Lü et al. (2008)	3.0 ± 0.3	Coe-Graphite	570–630	Coe-Graphite	(3)
Lü et al. (2009)	>2.5–2.9	Coe-Qtz	420–520	Grt-Cpx[b]	(4)
Beinlich et al. (2010)	2.0 ± 0.2	Grt-Cpx-Phen	480–540	Grt-Cpx[b]	(5)
Present study	2.1 ± 0.2	Grt-Cpx-Phen	540–600	Grt-Cpx[b]	(6)
Present study	1.8 ± 0.2	Grt-Cpx-Phen	500–580	Grt-Cpx[b]	(6)
Present study	1.7 ± 0.2	Grt-Cpx-Phen	330–430	Grt-Cpx[b]	(6)
Quantitative phase diagrams					
Klemd et al. (2002)	1.8–2.1		490–570		(1)
Lü et al. (2007)	1.8–1.9		400–500		(7)
Lü et al. (2007)	2.0–2.4		540–600		(7)
Wei et al. (2009)	2.1–2.3		530–550		(8)
Wei et al. (2009)	2.8–3.2		500–570		(8)
Lü et al. (2009)	>2.5–2.7		470–510		(4)
Beinlich et al. (2010)	1.9–2.2		480–540		(5)

[a] Number of PT-estimate in Fig. 3.
[b] Fe3+ stoichiometrically calculated.

Table 3
Lu–Hf data for Tianshan high pressure rocks.

Sample	Lu ppm	Hf ppm	$^{176}Lu/^{177}Hf$	Est. % 2 s.d.	$^{176}Hf/^{177}Hf$	±2 s.e. in 6th digit	Est. % 2 s.d.
Mafic meta-volcanic rock							
FTS 9-3							
wr bomb	0.514	6.36	0.01147	0.25	0.282698	(4)	0.0032
wr bomb replicate	–	6.36	–	–	0.282692	(7)	0.0052
omp-1	0.154	2.24	0.009805	0.28	0.282675	(6)	0.0048
grt-1	2.08	1.61	0.1833	0.25	0.283694	(6)	0.0048
grt-2	2.08	1.49	0.1990	0.25	0.283800	(7)	0.0052
Meta-volcaniclastic rocks							
FTS 9-2							
wr bomb	0.306	4.11	0.01055	0.25	0.282634	(6)	0.0044
wr chips tt	0.381	1.30	0.04149	0.25	0.282826	(6)	0.0048
omp-1 tt	0.0144	0.850	0.002409	0.31	0.282579	(7)	0.0052
grt-1 tt	1.22	0.971	0.1789	0.25	0.283627	(5)	0.0036
grt-1 tt replicate	–	0.970	–	–	0.283633	(5)	0.0036
grt-2 tt	1.32	0.861	0.2181	0.25	0.283864	(5)	0.0036
grt-3 tt	1.22	1.09	0.1583	0.25	0.283503	(5)	0.0036
grt-4 tt	1.34	0.962	0.1977	0.25	0.283745	(9)	0.0064
FTS 9-4							
wr bomb	0.400	2.31	0.02456	0.25	0.283191	(9)	0.0064
wr chips tt	0.388	0.587	0.09372	0.25	0.283625	(9)	0.0068
omp-1 tt	0.178	0.559	0.04527	0.30	0.283342	(12)	0.0088
grt-1 tt	2.14	1.01	0.2990	0.25	0.284814	(5)	0.0040
grt-2 tt	2.11	0.819	0.3666	0.25	0.285214	(6)	0.0044
grt-3 tt	2.12	0.850	0.3543	0.25	0.285150	(6)	0.0048
FTS 5-15							
wr bomb 1	0.315	1.64	0.02729	0.25	0.283110	(6)	0.0048
wr bomb 2	0.299	1.70	0.02496	0.25	0.283105	(7)	0.0052
wr chips tt	0.161	0.270	0.08489	0.25	0.283510	(11)	0.0084
matrix bomb	0.167	1.73	0.01366	0.26	0.283032	(7)	0.0056
grt-1 tt	1.35	0.305	0.6274	0.25	0.286641	(16)	0.0116
grt-2 tt	1.26	0.240	0.7446	0.25	0.287356	(6)	0.0048
grt-3 tt	1.43	0.181	1.119	0.25	0.289529	(7)	0.0052
grt-4 tt	1.41	0.225	0.8934	0.25	0.288247	(5)	0.0040
grt-5 tt	1.32	0.264	0.7113	0.25	0.287143	(5)	0.0036
grt-6 tt	1.20	0.274	0.6213	0.25	0.286621	(8)	0.0060
grt-7 tt	1.28	0.277	0.6541	0.28	0.286860	(13)	0.0092

Abbreviations: "replicate" denotes solutions that were analyzed twice for Hf. "wr" = powdered whole rock,"grt" = garnet, "omp" = omphacite, "matrix" = mineral grains remaining after extracting most garnet. "bomb"= sample digested in a high pressure autoclave, "tt" = tabletop digestion method in Teflon vials. "est. % 2 s.d." denotes the estimated external reproducibilities (i.e., 2 standard deviations, in %) of 176Lu/177Hf and 176Hf/177Hf. The former includes error magnification due to any sub-optimal spiking; the latter is based upon the method of Bizzarro et al. (2003). See text for further details. The absolute 2 s.e. (standard error) uncertainties of the 176Hf/177Hf analyses are also shown.

et al., 2005) from the same vicinities. The rapid transition from prograde garnet growth to retrograde mica (re-) crystallization indicates fast initial exhumation rates. The Lu–Hf ages are identical to the Grt Sm–Nd age of 343 ± 44 Ma (Gao and Klemd, 2003) that until now represented the only age for the prograde growth of an eclogite-facies mineral assemblage in this area.

The consistent Lu–Hf ages for high-pressure rocks that come from different depths with different P-T conditions, and their agreement with Sm–Nd ages from other parts of the Tianshan show that high-pressure metamorphism in the Tianshan occurred at ca. 315 Ma and was followed by fast exhumation as indicated by white mica cooling ages between 313 and 302 Ma (Klemd et al., 2005).

8.2. Slabs kinked at depth

We tentatively relate the exhumation of the oceanic HP and UHP eclogite boudins to that of the enclosing buoyant meta-sediments as was suggested for eclogites from the Western Alps (Agard et al., 2009). Such a scenario is supported by the intimate interlayering of HP and UHP eclogites with metasediments (Lü et al., 2007, 2008, 2009; Wei et al., 2009) as well as the occurrence of prograde blueschists and eclogites (e.g., Gao et al., 2007; John et al., 2008; Beinlich et al., 2010, present study) that were presumably plucked from different depths by buoyant metasediments and raised quickly enough to shallow crustal levels to escape significant re-equilibration during the exhumation process. The peak metamorphic P-T estimates of the UHP eclogites all lie on a colder P-T path than those of the HP eclogites (Fig. 3). This is probably not the result of sampling different depths of the slab stratigraphy because these rocks are all closely associated with prograde HP and UHP host metasediments (Wei et al., 2009) and frequently preserve pillow structures (e.g., Gao and Klemd, 2003), suggesting they were all derived from the uppermost oceanic crust, i.e., at or near the slab interface. Furthermore, the peak P-T estimates of the host HP and UHP metasediments also lie on the two distinct P-T trajectories (Fig. 3). This behavior is probably not caused by inconsistencies between the thermobarometry results of HP and UHP metasediments because both were investigated with the same thermodynamic modeling approach, the same computer software, and the same internally consistent thermodynamic datasets (Wei et al., 2009).

Remaining ways to explain the close intermingling of HP and UHP rocks include: 1) juxtaposition processes during subduction and exhumation within the subduction channel, 2) variations in the slab convergence rate, and 3) a change in the slab geometry, i.e. a sudden change in the slab dip at great depth ('kinking'). Relevant to scenario 1, some numerical modeling studies (Gerya et al., 2002; Gerya et al., 2008; Gerya and Stöckhert, 2006) suggest that HP and UHP mafic oceanic crust followed different P-T paths within single subduction zones. Modeled P-T trajectories for particles (rocks) from different depths within and above the slab interface or particles *which had 'left' the slab interface before reaching UHP conditions* (i.e., *during subduction*), display several dissimilar prograde (and retrograde) P-T trajectories. Such models would predict that some of the HP rocks investigated here should conform to the cold P-T trajectory (lower geothermal gradient) and/or some UHP rocks with the warm P-T trajectory (higher geothermal gradient), or perhaps that all rocks would all lie on different P-T trajectories (Gerya and Stöckhert, 2006). Instead, peak P-T estimates of the Tianshan UHP metasediments and eclogites all lie on a 'colder' P-T path than the HP eclogites and metasediments (Fig. 3). Furthermore, the aforementioned model applies only to rocks derived from different depths within the subducting slab section, but, as mentioned above, the Tianshan HP and UHP eclogites and metasediments seem to have been restricted to near the slab's surface. In scenario 2, a change in the convergence rate during subduction could also generate different P-T trajectories in a single slab (e.g., Peacock et al., 2005). Again, if this were the case, one would still expect to find some HP rocks on the lower geothermal gradient and/or some UHP rocks on the higher geothermal gradient. Also, the P-T trajectories of subducting slabs are rather insensitive to modest variations in convergence rate (e.g., Peacock et al., 2005). Therefore, the substantially different peak metamorphic P-T estimates of the UHP metasediments and eclogites, which all lie on a 'colder' P-T path than the HP eclogites and metasediments (Fig. 3), cannot be explained by change in the convergence rate alone.

According to the evolution of the slab surface temperature in subduction zones, the deeper "released" sample should have a higher temperature at the highest pressure (e.g., Plank et al., 2009; Syracuse et al., 2010). Consequently, we interpret the different P-T trajectories required by the intercalated HP and UHP eclogites and metasediments to indicate a sharp increase in the dip angle of the subducted slab (scenario 3) between the depths at which HP and UHP conditions are reached, i.e., near 90 km depth. Wadati–Benioff seismicity profiles suggest that such an inflection indeed occurs in some subduction zones, for instance along the convergent margins of the Americas (Fig. 5). This finding is supported by detailed receiver function imaging of the Alaska (Rondenay et al., 2008), Cascadia (Rondenay et al., 2001; Rondenay et al., 2008, Abers et al. 2009), Nicaragua (MacKenzie et al., 2010), and Chilean (Yuan et al., 2000) subduction zones.

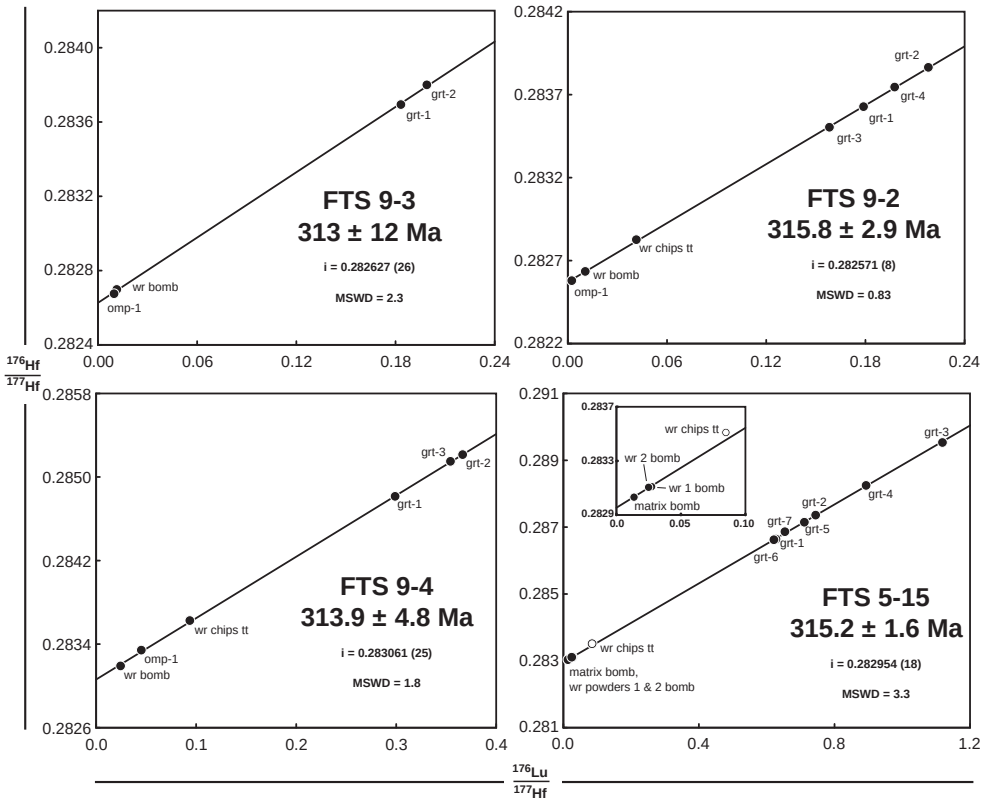

Fig. 4. Lu–Hf garnet-whole-rock isochrons for high-pressure rocks from the Chinese Tianshan HP-LT belt. All fractions were included in the regressions except the wr chips tt (= tabletop digestion) from sample FTS 5-15 (open circle).

Such kinks are not ubiquitous, but they are found in several subduction zones worldwide, often coinciding with the disappearance of the low-velocity subducted oceanic crust at depth. This is the point where eclogitization (dehydration) of the upper oceanic crust (including drier gabbroic parts) is thought to be nearly complete and the oceanic crust becomes almost seismically indistinguishable from mantle peridotite (e.g., Rondenay et al., 2001; Rondenay et al., 2008; van Keken et al., 2011; Yuan et al., 2000). A coincident increase in subduction angle may stem from a greater slab pull resulting from the densification that accompanies eclogitization. It may additionally be facilitated by temporary weakening of the slab in response to eclogitization reactions (e.g., Austrheim, 1987; John et al., 2009; Jolivet et al., 2005). We hypothesize that this reaction activity, brief weakening, and deformation are most intense where the slab loses its low velocity layer (e.g., Fig. 2c in Yuan et al., 2000). Just after this point, the slab is denser and has regained its strength. The depth of this critical point at which the low-velocity subducted crust disappears varies among subduction zones (Fig. 5; e.g., Yuan et al., 2000; Rondenay et al., 2008). In the Tianshan, we find that a kink marking the transition in geothermal gradients between UHP and HP rocks would have occurred at ~90 km depth. This is similar to the kink observed beneath the Central Andes (e.g., Yuan et al., 2000), but much deeper than that of the Cascadia subduction zone (Rondenay et al., 2001; Rondenay et al., 2008). This variation in kink depth observed among subduction zones of the same collisional type (oceanic-continental), suggests that factors such as geometry and thermal structure are involved: The subducting plate in the Central Andes is significantly older than that in Cascadia, i.e., ~46 vs. ~10 Ma, and its convergence rate is twice as fast, i.e., ~79 mm/yr vs. ~40 mm/yr. Additionally, the initial slab dips are 30° and 22°, respectively (Syracuse et al., 2010, and references therein). Given that the blueschist–eclogite transformation occurred at 50–70 km depth in the former Tianshan subduction zone (see above), the kink depth seems to be not only a function of slab dehydration, but also of the later availability of fluids that catalyze the metamorphic reactions, thereby inducing eclogitization within the drier or even unaltered (gabbroic) parts of the interior of the subducting oceanic crust at depth (e.g., Austrheim, 1987; John and Schenk, 2003; Putnis and John, 2010; Rubie, 1998; van Keken et al., 2011). Accordingly, we interpret the kink depth to be a function of the age of the oceanic slab, its subduction rate, and its initial dip. To a first order, these parameters should control when and where slab dehydration and kinetically delayed (but fluid-triggered) metamorphic reactions occur in the subducting plate.

The kinking feature thus has important implications for the descent of slabs and for determining which parts of them can eventually exhume. Apart from the negative buoyancy of mafic UHP rocks, the kinking in subduction zones may act as an additional (geometric) hindrance that the rocks must overcome during exhumation from subducting oceanic plates. For example, one consequence of the kink might be that the transporting matrix in the subduction channel pinches out at the kink, inhibiting exhumation of rocks from greater depth. This may explain why oceanic crust from such depths is exceedingly rare: As of yet, it has only been reported from the Tianshan. In contrast to mafic oceanic crust, continental crust does not undergo any large-scale hydration before subduction and thus remains stiff and unkinked during subduction (e.g., Andersen et al., 1991; Jackson et al., 2004). The positive buoyancy of such crust and the lack of a geometric exhumation hindrance may explain the more common occurrence of UHP rocks within large, coherent slices of continental slabs.

Supplementary materials related to this article can be found online at doi: 10.1016/j.epsl.2011.07.022.

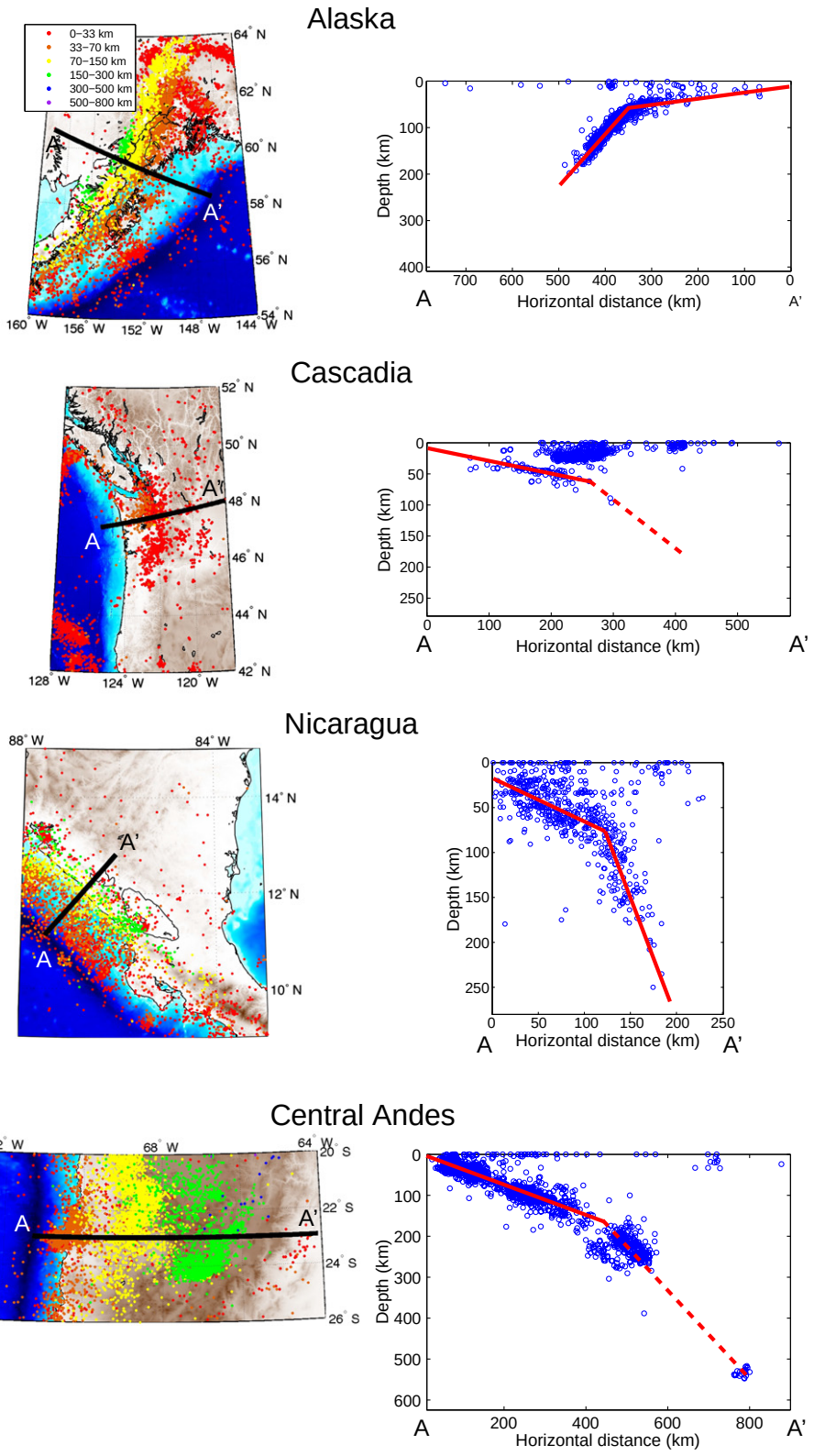

Fig. 5. Maps and profiles of seismicity across subduction zones spanning the west coast of the Americas: Alaska, Cascadia, Nicaragua, and the central Andes. Hypocenters were obtained through a combined search of NEIC and ISC catalogs using the IRIS event query tool (http://www.iris.edu/SeismiQuery/sq-events.htm). Left panels show seismicity (M>2) in map view for periods between 01/01/2000-01/01/2011 in Alaska, Nicaragua, central Andes, and 01/01/1980-01/01/2011 in Cascadia. Earthquakes are color-coded as a function of depth range (see inset). Right panels show depth profiles of seismicity in each region for events located within +/− 50 km of projection lines (A–A′) displayed on the maps. Red lines drawn through the centers of the Wadati–Benioff zones schematically illustrate the kink in each of the subducted slabs.

Acknowledgments

We are grateful to Heidi Baier for keeping Münster's isotope laboratory running smoothly. We thank J. Berndt for support during the LA–ICP-MS work and the microprobe mapping in Münster. I. Osbahr is thanked for help with the microprobe analyses in Erlangen. The study was supported by the Deutsche Forschungsgemeinschaft (KL 17-1,2,3) and the 'National Basic Research program of China' (2007CB411302 and 2001CB409803). Stéphane Rondenay is supported by NSF grants Continental Dynamics EAR-0409373 and Earthscope EAR-0544996. Taras Gerya and an unknown referee are thanked for constructive reviews.

References

Abers, G.A., MacKenzie, L.S., Rondenay, S., Zhang, Z., Wech, A.G., Creager, K.C., 2009. Imaging the source region of Cascadia tremor and intermediate-depth earthquakes. Geology 37, 1119–1122.

Abers, G.A., 2005. Seismic low velocity layer at the top of subducting slabs beneath volcanic arcs: observations, predictions, and systematics. Phys. Earth Planet. Inter. 149, 7–29.

Agard, P., Yamato, P., Jolivet, L., Burov, E., 2009. Exhumation of oceanic blueschists and eclogites in subduction zones: timing and mechanisms. Earth Sci. Rev. 92, 53–79.

Andersen, T.B., Jamtveit, B., Dewey, J.F., Swensson, E., 1991. Sub-duction and eduction of continental crust: major mechanisms during continent–continent collision and orogenic extensional collapse, a model based on the south Norwegian Caledonides. Terra Nova 3, 303–310.

Austrheim, H., 1987. Eclogitization of lower crustal granulites by fluid migration through shear zones. Earth Planet. Sci. Lett. 81, 221–232.

Beinlich, A., Klemd, R., John, T., Gao, J., 2010. Trace-element mobilization during Ca-metasomatism along a major fluid conduit: eclogitization of blueschist as a consequence of fluid–rock interaction. Geochim. Cosmochim. Acta 74, 1892–1922.

Bizzarro, M., Baker, J.A., Haack, H., Ulfbeck, D., Rosing, M., 2003. Early history of Earth's crust-mantle system inferred from hafnium isotopes in chondrites. Nature 421 (6926), 931–933.

Blichert-Toft, J., Boyet, M., Telouk, P., Albarède, F., 2002. ^{147}Sm–^{143}Nd and ^{176}Lu–^{176}Hf in eucrites and the differentiation of the HED parent body. Earth Planet. Sci. Lett. 204, 167–181.

Carswell, D.A., 1990. Eclogite Facies Rocks. Blackie, Glasgow.

Clarke, G.L., Powell, R., Fitzherbert, J.A., 2006. The lawsonite paradox: a comparison of field evidence and mineral equilibria modelling. J. Metamorph. Geol. 24, 715–725.

Ellis, D.J., Green, D.H., 1979. An experimental study of the effect of Ca upon garnet-clinopyroxene Fe–Mg exchange equilibria. Contrib. Mineral. Petrol. 71, 72–80.

Evans, B.W., 1990. Phase relations of epidote-blueschists. Lithos 25, 3–23.

Gao, J., Klemd, R., 2003. Formation of HP-LT rocks and their tectonic implications in the western Tienshan Orogen, NW China: geochemical and age constraints. Lithos 66, 1–22.

Gao, J., He, G., Li, M., Tang, Y., Xiao, X., Zhou, M., 1995. The mineralogy, petrology, metamorphic PTDt trajectory and exhumation mechanism of blueschists, South Tianshan, northwestern China. Tectonophysics 250, 151–168.

Gao, J., Li, M., Xiao, X., Tang, Y., He, G., 1998. Paleozoic tectonic evolution of the Tianshan orogen, northwestern China. Tectonophysics 287, 213–231.

Gao, J., Klemd, R., Zhang, L., Wang, Z., Xiao, X., 1999. P-T path of high pressure/low temperature rocks and tectonic implications in the western Tianshan Mountains, NW China. J. Metamorph. Geol. 18, 621–636.

Gao, J., John, T., Klemd, R., Xiong, X., 2007. Mobilization of Ti–Nb–Ta during subduction: evidence from rutile-bearing dehydration segregations and veins hosted in eclogite, Tianshan, NW-China. Geochim. Cosmochim. Acta 71, 4974–4996.

Gerya, T.V., Stöckhert, B., 2006. Two-dimensional numerical modeling of tectonic and metamorphic histories at active continental margins. Int. J. Earth Sci. 95, 250–274.

Gerya, T.V., Stöckhert, B., Perchuk, A.L., 2002. Exhumation of high-pressure metamorphic rocks in a subduction channel: a numerical simulation. Tectonics 21 Article No. 1056.

Gerya, T.V., Perchuk, L.L., Burg, J.-P., 2008. Transient hot channels: perpetrating and regurgitating ultrahigh-pressure, high-temperature crust–mantle associations in collision belts. Lithos 103, 236–256.

Hegner, E., Klemd, R., Kröner, A., Corsini, M., Alexeiev, D.V., Iaccheri, L.M., Zack, T., Dulski, P., Xia, X., Windley, B.F., 2010. Mineralogy, ages and P-T conditions of late Paleozoic high-pressure eclogite and provenance of mélange sediments in the South Tianshan Orogen of Kyrgyzstan. Am. J. Sci. 310, 916–950.

Holland, T.J.B., 1980. The reaction albite = jadeite + quartz determined experimentally in the range 600–1200 °C. Am. Mineral. 65, 129–134.

Hollister, L.S., 1966. Garnet zoning: an interpretation based on the Rayleigh fractionation model. Science 154, 1147–1150.

Jackson, J.A., Austrheim, H., McKenzie, D., Priestley, K., 2004. Metastability, mechanical strength, and the support of mountain belts. Geology 32, 625–628.

Jochum, K. P., Stoll, B., Herwig, K., Willibold, K.,; Hofmann, A.W., et al., 2006. MPI-DING Reference Glasses for In-Situ Microanalysis: New Reference Values for Element Concentrations and Isotope Ratios.: Geochem. Geophys. Geosyst. doi:10.1029/2005GC001060.

John, T., Schenk, V., 2003. Partial eclogitization of gabbroic rocks in a late Precambrian subduction zone (Zambia): prograde metamorphism triggered by fluid infiltration. Contrib. Mineral. Petrol. 146, 174–191.

John, T., Klemd, R., Gao, J., Garbe-Schönberg, C.D., 2008. Trace element mobilization in slabs due to non steady-state fluid–rock interaction: constraints from an eclogite-facies transport vein in blueschist (Tianshan, China). Lithos 103, 1–24.

John, T., Medvedev, S., Rüpke, L.H., Podladchikov, Y., Andersen, T.B., Austrheim, H., 2009. Generation of intermediate-depth earthquakes by self-localizing thermal runaway. Nat. Geosci. 2, 137–140.

Jolivet, L., Raimbourg, H., Labrousse, L., Avigad, D., Leroy, Y., Austrheim, H., Andersen, T.B., 2005. Softening triggered by eclogitization, the first step toward exhumation during continental subduction. Earth Planet. Sci. Lett. 237, 532–547.

Klemd, R., Schröter, F.C., Will, T.M., Gao, J., 2002. P-T evolution of glaucophane-omphacite bearing HP-LT rocks in the western Tianshan Orogen, NW China: new evidence for Alpine-type tectonics. J. Metamorph. Geol. 20, 239–254.

Klemd, R., Bröcker, M., Hacker, B.R., Gao, J., Gans, P., Wemmer, K., 2005. New age constraints on the metamorphic evolution of the high-pressure/low-temperature belt in the western Tienshan mountains, NW China. J. Geol. 113, 157–168.

Krogh-Ravna, E., 2000. The garnet-clinopyroxene Fe^{2+}–Mg geothermometer: an updated calibration. J. Metamorph. Geol. 8, 211–219.

Lagos, M., Scherer, E.E., Tomaschek, F., Münker, C., Keiter, M., Berndt, J., Ballhaus, C., 2007. High precision Lu–Hf geochronology of Eocene eclogite-facies rocks from Syros, Cyclades. Greece. Chem. Geol. 243, 16–35.

Lapen, T.J., Johnson, C.M., Baumgartner, L.P., Mahlen, N.J., Beard, B.L., Amato, J.M., 2003. Burial rates during prograde metamorphism of an ultra-high-pressure terrane: an example from Lago di Cignana, western Alps, Italy. Earth. Planet. Sci. Lett. 215, 57–72.

Leake, B.E., 1978. Nomenclature of amphiboles. Am. Mineral. 63, 1023–1052.

Li, Z., Gerya, T.V., 2009. Polyphase formation and exhumation of HP–UHP rocks in continental subduction zones: numerical modelling and application to the Sulu UHP terrane in China. J. Geophy. Res. 114, B09406. doi:10.1029/2008JB005935.

Lin, W., Enami, M., 2006. Prograde pressure–temperature path of jadeite-bearing eclogites and associated high-pressure/low-temperature rocks from western Tianshan, northwest China. Isl. Arc 15, 483–502.

Lü, Z., Zhang, L.F., Qü, J.F., Li, H.F., 2007. Petrology and metamorphic P-T path of eclogites from Habutengsu, southwestern Tianshan, Xinjiang. Acta Petrol. Sin. 23, 1617–1626.

Lü, Z., Zhang, L., Du, J., Bucher, K., 2008. Coesite inclusions in garnet from eclogitic rocks in western Tianshan, northwest China: convincing proof of UHP metamorphism. Am. Mineral. 93, 1845–1850.

Lü, Z., Zhang, L.F., Du, J., Bucher, K., 2009. Petrology of coesite-bearing eclogite from Habutengsu Valley, western Tianshan, NW China and its tectonometamorphic implication. J. Metamorph. Geol. 27, 773–787.

Ludwig, K.R., 2008. Isoplot/Ex 3.70, A geochronological toolkit for Microsoft Excel. Berkeley Geochronology Center Special Publication No. 4.

MacKenzie, L.S., Abers, G.A., Rondenay, S., Fischer, K.M., 2010. Imaging a steeply dipping subducting slab in Southern Central America. Earth Planet. Sci. Lett. 296, 459–468.

Morimoto, N., Fabries, J., Ferguson, A.K., Ginzburg, I.V., Ross, M., Seifert, F.A., Zussman, J., Aoki, K., Gottardi, G., 1988. Nomenclature of pyroxene. Am. Mineral. 73, 1123–1133.

Münker, C., Weyer, S., Scherer, E.E., Mezger, K., 2001. Separation of high field strength elements (HFSE) and Lu from rock samples für MC–ICPMS measurements. Geochim. Geophys. Geosyst. 2. doi:10.1029/2001GC000183.

Otamendi, J.E., de la Rosa, J.D., Patino Douce, A.E.P., Castro, A., 2002. Rayleigh fractionation of heavy rare earths and yttrium during metamorphic garnet growth. Geology 30, 159–162.

Peacock, S.M., van Keken, P.E., Holloway, S.D., Hacker, B.R., Abers, G.A., Fergason, R.L., 2005. Thermal structure of the Costa Rica–Nicaragua subduction zone. Phys. Earth Planet. Inter. 149, 187–200.

Pearce, N.J.G., Perkins, W.T., Westgate, J.A., Gorton, M.P., Jackson, S.E., Neal, C.R., Chenery, S.P., 1997. A compilation of new and published major and trace element data for NIST SRM 610 and NIST SRM 612 glass reference materials. Geostand. Newslet - J. Geostand. Geoanalysis 21 (1), 115–144.

Plank, T., Cooper, L.B., Manning, C.E., 2009. Emerging geothermometers for estimating slab surface temperatures. Nat. Geosci. doi:10.1038/NGE0614

Putnis, A., John, T., 2010. Replacement processes in the Earth's crust. Elements 6, 159–164.

Ravna, E.J.K., Andersen, T.B., Jolivet, L., DeCapitani, C., 2010. Cold subduction and the formation of lawsonite eclogite—constraints from prograde ecolution of eclogitized pillow lava from Corsica. J. Metamorph. Geol. 28, 381–395.

Rondenay, S., Bostock, M.G., Shragge, J., 2001. Multiparameter two-dimensional inversion of scattered teleseismic body waves 3. Application to the Cascadia 1993 data set. J. Geophys. Res. 106, 30795–30807.

Rondenay, S., Abers, G.A., van Keken, P.E., 2008. Seismic imaging of subduction zone metamorphism. Geology 36, 275–278.

Rubie, D.C., 1998. Disequilibrium during metamorphism: the role of nucleation kinetics. In: Treloar, P.J., O'Brien, P.J. (Eds.), What drives metamorphism and metamorphic reactions? : Geol. Soc. Spec. Publ. London, 138, pp. 199–214.

Scherer, E.E., Cameron, K.L., Blichert-Toft, J., 2000. Lu–Hf garnet geochronology: closure temperature relative to the Sm–Nd system and the effects of trace mineral inclusions. Geochim. Cosmochim. Acta 64, 3413–3432.

Scherer, E., Münker, C., Mezger, K., 2001. Calibration of the lutetium-hafnium clock. Science 293, 683–687.

Scherer, E.E., Mezger, K., Münker, C., 2003. The ^{176}Lu decay constant discrepancy: terrestrial samples versus meteorites. Meteor. Planet. Sci. 38 (N7, Supplement), A136.

Schulz, B., Klemd, R., Brätz, H., 2006. Host rock compositional controls on zircon trace element signatures in metabasites from the Austroalpine basement. Geochim. Cosmochim. Acta 70, 697–710.

Sengör, A.M.C., Natal'in, B.A., Burtman, V.S., 1993. Evolution of the Altaid tectonic collage and Paleozoic crustal growth in Eurasia. Nature 364, 299–307.

Simonov, V.A., Sakiev, K.S., Volkova, N.I., Stupakov, S.I., Travin, A.V., 2008. Conditions of formation of the Atbashe Ridge eclogites (South Tianshan). Russian Geol. Geophys. 49, 803–815.

Söderlund, U., Patchett, P.J., Vervoort, J.D., Isachsen, C.E., 2004. The ^{176}Lu decay constant determined by Lu–Hf and U–Pb isotope systematics of Precambrian mafic intrusions. Earth Planet. Sci. Lett. 219, 311–324.

Sprung, P., Scherer, E.E., Upadhyay, D., Leya, I., Mezger, K., 2010. Non-nucleosynthetic heterogeneity in non-radiogenic stable Hf isotopes: Implications for early solar system chronology. Earth Plan. Sci. Lett. 295, 1–11.

Stupakov, S.I., Volkova, N.I., Travin, A.V., Simonov, A., Sakiev, K.S., Novgorodtsev, O.S., 2004. Eclogites of Atbashi Ridge as indicators of Early Carboniferous collision in Southern Tien Shan. In: Chernyshov, A.I., Tishin, P.A., Bether, O.V., Vrublevsky, V.V., Gertner, I.F., Grinev, O.M., Krasnova, T.S. (Eds.), Petrology of magmatic and metamorphic complexes: Issue 4, Tomsk Center for Scientific and Technical Information, pp. 272–277.

Su, W., Gao, J., Klemd, R., Li, J.L., Zhang, X., Li, X.H., Chen, N.S., Zhang, L., 2010. U–Pb zircon geochronology of the Tianshan eclogites in NW China: implication for the collision between the Yili and Tarim blocks of the southwestern Altaids. Eur. J. Mineral. 22, 473–478.

Syracuse, E.M., van Keken, P.E., Abers, G.A., 2010. The global range of subduction zone thermal models. Phys. Earth Planet. Int. 51, 1761–1782.

van der Straaten, F., Schenk, V., John, T., Gao, J., 2008. Blueschist-facies rehydration of eclogites (Tian Shan, NW-China): implications for fluid–rock interaction in the subduction channel. Chem. Geol. 255, 195–219.

Van Keken, P.E., Hacker, B.R., Syracuse, E.M., Abers, G.A., 2011. Subduction factory: 4. Depth-dependent flux of H2O from subducting slabs worldwide. J. Geophys. Res. 116, BO41401. doi:10.1029/2010/JB007922.

Van Orman, J.A., Grove, T.L., Shimizu, N., Layne, G.D., 2002. Rare earth element diffusion in a natural pyrope single crystal at 2.8 GPa. Contrib. Mineral. Petrol. 142, 416–424.

Warren, C.J., Beaumont, C., Jamieson, R.A., 2008a. Modelling tectonic styles and ultra-high pressure (UHP) rock exhumation from oceanic subduction to continental collision. Earth Planet. Sci. Lett. 267, 129–145.

Warren, C.J., Beaumont, C., Jamieson, R.A., 2008b. Formation and exhumation of ultra-high-pressure rocks during continental collision: role of detachment in the subduction channel. Geochem. Geophy. Geosys. 9. doi:10.1029/2007GC001839.

Waters, D.J., 1996. The Garnet-Cpx-phengite barometer. http://www.earth.ox.ac.uk 1996.

Wei, C., Wang, B., Clarke, G.L., Zhang, L., Song, S., 2009. Metamorphism of high/ultrahigh-pressure pelitic–felsic schist in the south Tianshan orogen, NW China: phase equilibria and P–T path. J. Petrol. 50, 1973–1991.

Yamato, P., Burov, E., Agard, P., Le Pourhiet, L., Jolivet, L., 2007. Burial and exhumation in a subduction wedge: mutual constraints from thermomechanical modeling and natural P-T-t data (Schistes Lustres, western Alps). J. Geophys. Res. 112, B07410. doi:10.1029/2006JB004441.

Yuan, X., Sobolev, S.V., Kind, R., Oncken, O., Bock, B., Asch, G., et al., 2000. Subduction and collision processes in the Central Andes constrained by converted seismic phases. Nature 408, 958–961.

Zhang, L.F., Ai, Y.L., Li, X.P., Rubatto, D., Song, B., Williams, S., Song, S.G., Ellis, D., Liou, J.G., 2007. Triassic collision of western Tianshan orogenic belt, China: Evidence from SHRIMP U-Pb dating of zircon from HP/UHP eclogitic rocks. Lithos 96 (1–2), 266–280.

Zonenshain, L.P., Kuzmin, M.I., Natapov, L.M., 1990. Geology of the USSR: a plate-tectonic synthesis. In: Page, B.M. (Ed.), Am. Geophys. Union, Geody. Series, 21. 242 p.